Circuit Conditions to Prevent Second-Subharmonic Power Extraction in Periodically Driven IMPATT Diode Networks

DEAN F. PETERSON, MEMBER, IEEE

Abstract—**The small-signal characteristics at the second subharmonic (half-frequency) of a periodically pumped IMPATT diode are presented. Theoretical analysis using an appropriate model indicates these characteristics can be interpreted as a "phase-sensitive admittance" which clarifies subharmonic oscillation conditions and suggests a method for their measurement. Measured data on silicon and GaAs diodes de-embedded to the active wafer are in good agreement with theoretical predictions based on the equivalent nonlinear model for each device. Circuit conditions that eliminate second subharmonics and thus prevent fundamental power robbing are given which can be readily obtained for existing devices. An example demonstrating the efficiency-limiting properties of subharmonics is given.**

I. INTRODUCTION

THE POSSIBILITY of subharmonic generation or harmonic division in networks containing periodically pumped nonlinear energy storage elements is well known from varactor theory [1]. These parametric oscillations can also exist, under certain conditions, in IMPATT diode networks when the nonlinear inductance of the avalanche process [2]–[4] is driven at large signal. Snapp [5] was able to achieve efficient power generation below the avalanche frequency at the second subharmonic (half-frequency) of an IMPATT oscillator in a manner not related to the TRAPATT mode. Schroeder and Haddad [6] showed that induced negative conductance and thus oscillations could occur at a second subharmonic below the avalanche frequency, but only for certain phase angles of the subharmonic relative to the fundamental.

The presence of this oscillation in high-power IMPATT amplifiers and oscillators is often observed and will usually impose an unnecessary limitation on the power available at the fundamental. Subharmonic generation is a threshold phenomenon and its effect on IMPATT amplifiers is seen as a sharp decrease in added power and output power when the drive power is increased above the threshold level. As will be shown by example, this can limit the diode generation efficiency if the threshold occurs at an added power level below the maximum [7], [8]. Normally, the second subharmonic is most easily generated since it does not require an idler to start (small signal), while all higher order subharmonics require idlers to exist [1]. In this paper we determine, both theoretically and experimentally, the circuit conditions which will prevent this oscillation so that the full power capability of the IMPATT can be realized. Hines [4], in a recent in-depth study of IMPATT parametric effects, proposed that the circuit impedance at the second subharmonic should have a low resistance and finite inductive component to avoid oscillation. Although this result is verified here (for low inductances), it is further shown that many other types of circuit behavior are effective in eliminating second subharmonics.

In Section II a small-signal analysis of a pumped IMPATT using an appropriate model of the nonlinearity [3], [4], [9] leads directly to device subharmonic oscillation threshold conditions expressed in terms of measurable device parameters [10]. The analysis is similar to that given in [4], but the subharmonic behavior is straightforwardly derived and interpreted in terms of a "phase-sensitive admittance" which clarifies oscillation conditions and suggests a consistent method of measuring this characteristic. The measurement technique and results are described in Section III for K_a-band (36–40-GHz) silicon and GaAs diodes. Appropriate parameters for the nonlinear model are determined for these devices from small-signal unpumped data in accordance with [10]. The resulting theoretical predictions of subharmonic characteristics are compared to measured data with substantial quantitative agreement. This result indicates that circuits for prevention of subharmonics can be appropriately designed through knowledge of a few simply determined device parameters.

II. PREDICTION AND INTERPRETATION OF SUBHARMONIC PROPERTIES OF A PUMPED IMPATT DIODE

The subharmonic oscillation conditions are developed using the two-zone Read model for the IMPATT diode. The electric field in this ideal device will consist of a thin high-field region in which both carrier generation (ionization) and drift occur and a lower field region where carriers drift at saturated velocities but do not ionize. It has been assumed in the following analysis that holes and electrons have equal ionization rates and that their drift velocities are equal. The saturation current is also neglected.

The nonlinear properties of the IMPATT primarily arise through the high sensitivity of the ionization rate α on the electric field. Using a linear approximation for the variation of α with field, Evans and Haddad [3] have given a nonlinear analysis for this device which allows the terminal

Manuscript received November 26, 1973; revised February 7, 1974. This work was sponsored by the Department of the Air Force.
The author is with the Massachusetts Institute of Technology, Lincoln Laboratory, Lexington, Mass. 02173.

voltage v_D and terminal current i_D to be expressed in terms of the avalanche-generated particle current $i_L(t)$ injected into the drift zone. Combining [3, eqs. (20) and (31)] and rearranging [9], one obtains

$$v_D - V_B = \frac{\Upsilon}{2\alpha'}\frac{1}{i_L}\frac{di_L}{dt} + \frac{l}{\epsilon \Upsilon A}\int_{t-\Upsilon}^{t} (\Upsilon - t + \sigma) i_L(\sigma)\, d\sigma \tag{1}$$

where α' is the electric-field derivation of α evaluated at the critical field, l is the drift-region length, A is diode area, and Υ is the carrier transit time in the drift region (the drift time in the avalanche zone is neglected). Thus the diode terminal voltage above the breakdown voltage V_B consists of a nonlinear component

$$v_L(t) = \frac{\lambda_0}{i_L(t)}\frac{di_L(t)}{dt} \tag{2a}$$

caused by ionization in the avalanche zone, and a linear component

$$v_R(t) = \frac{1}{\Upsilon C}\int_{t-\Upsilon}^{t} (\Upsilon - t + \sigma) i_L(\sigma)\, d\sigma \tag{2b}$$

caused by the space charge of the carriers in the drift zone, where $\lambda_0 \triangleq \Upsilon/2\alpha'$ and $C \triangleq \epsilon A/l$ is very nearly the total diode depletion capacitance, neglecting the avalanche region width. For slow variations in $i_L(t)$ with respect to Υ. Equation (2b) gives the space-charge resistance as $v_R \to (\Upsilon/2C) i_L$.

The diode terminal current i_D at time t consists of a conduction current component influenced by all the carriers injected into the drift zone from $t - \Upsilon$ to t plus the displacement current and is written as [3]

$$i_D(t) = C\frac{dv_D}{dt} + \frac{1}{\Upsilon}\int_{t-\Upsilon}^{t} i_L(\sigma)\, d\sigma. \tag{3}$$

The diode model we use is described by (1)–(3), these giving the terminal quantities in terms of the particle current parameter $i_L(t)$. It was shown in [9] that such a model with suitably determined values[1] for λ_0, Υ, and C give a good description of existing IMPATT devices, at least for short transit times. The nonlinearity in the model is given by (2a) and $v_L(t)$ can be described as the voltage across a nonlinear inductance $\lambda_0/i_L(t)$. This lossless energy storage element will be responsible for the parametric effects, in particular the subharmonic oscillation.

We wish to determine the device and circuit conditions which will result in the onset of a subharmonic oscillation. Accordingly, we let the quantities i_L and v_L be the sum of general pumping terms $i_p(t)$ and $v_p(t)$ periodic at $2\pi/\omega_p$ and small-signal perturbations i_l and v_l in order to linearize (2a) for incremental signal analysis. Since v_L is nonlinear in i_L, we can write

$$v_L = v_P + v_l = \frac{\lambda_0}{i_p + i_l}\frac{d}{dt}(i_p + i_l)$$

$$\cong \frac{\lambda_0}{i_p}\frac{di_p}{dt} + \frac{d}{dt}\left(\frac{\lambda_0}{i_p} i_l\right) \tag{4}$$

or

$$v_p(t) = \frac{\lambda_0}{i_p(t)}\frac{di_p(t)}{dt} \tag{5}$$

and

$$v_l(t) = \frac{d}{dt}\left(\frac{\lambda_0}{i_p(t)} i_l(t)\right) = \frac{d\lambda_l(t)}{dt} \tag{6}$$

where $\lambda_l \triangleq (\lambda_0/i_p) i_l$ may be regarded as the incremental flux variation in the nonlinear inductor under pumped conditions. The small-signal relation (6) describes the interaction of the small-signal variables i_l and v_l with the large-signal periodic pumping characterized by the "time-varying inductance" $\lambda_0/i_p(t)$. Using (6) with (1)–(3), the small-signal time-varying system can be represented as in the circuit of Fig. 1 from which parametric oscillation thresholds can be determined. The lowercase subscripts indicate small-signal quantities.

We are looking for circuit and pumping conditions to allow steady-state source-free voltages and currents periodic at $4\pi/\omega_p$ to exist in the network. The desired periodic solution will generally contain harmonic terms at $\omega_0 = \omega_p/2$, $3\omega_0$, $5\omega_0$, as these terms mixing with the pump will produce terms at the consistent set of frequencies $n\omega_p \pm \omega_0$. The solution can be considerably simplified if v_l contains a component only at ω_0 and the higher frequency *voltage* components are zero. This assumption is justified if the impedance $Z(j\omega)$ of the circuit to the *left* of the time-varying inductor in Fig. 1 (including the external circuit) approaches zero at $3\omega_0, 5\omega_0, \cdots$. Evaluating this impedance we find

$$Z(j\omega) = \frac{1}{j\omega C}\left\{1 - \left[\frac{1 - \exp(-j\omega\Upsilon)}{j\omega\Upsilon}\left(\frac{1}{1 + j\omega C Z_c}\right)\right]\right\} \tag{7}$$

where $Z_c(j\omega)$ is the external circuit impedance. We shall assume that $|Z_c| \to \infty$ at $n\omega_0$, $n = 3,5,\cdots$, and $n\omega_0 C$ is large enough such that the desired solution for $V_l(t)$ can be reasonably approximated as

$$v_l(t) = V_1 \exp(j\omega_0 t) + V_1^* \exp(-j\omega_0 t). \tag{8}$$

Using (8) we can now determine the circuit and pumping conditions under which this solution will be self-consistent.

The pumping current periodic at $2\pi/\omega_p$ is written as

$$i_p(t) = \sum_{-\infty}^{\infty} I_{pk} \exp(jk\omega_p t), \qquad I_{p-k} = I_{pk}^* \tag{9}$$

with I_{pk} the Fourier half-amplitudes. Substituting (8) and

[1] One can measure C and space-charge resistance $\Upsilon/2C$ low frequencies, and $\omega_a^2(I_{DC}) = 1/L(I_{DC})C$ can be determined from microwave measurements to give $L(I_{DC}) = \lambda_0/I_{DC}$, [10].

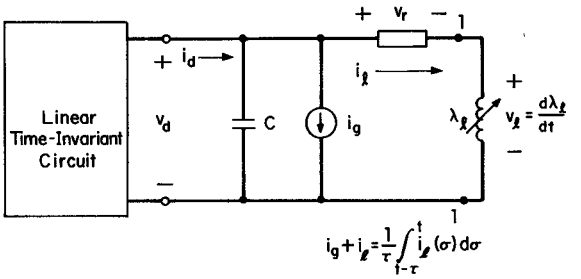

Fig. 1. An equivalent small-signal circuit model for a periodically pumped IMPATT diode.

(9) into (6) and writing $i_l(t)$ as

$$i_l(t) = \sum_{-\infty}^{\infty} I_k \exp(jk\omega_0 t), \qquad I_{-k} = I_k^* \tag{10}$$

we obtain for the half-amplitude current I_1 at $\omega_0 = \omega_p/2$

$$I_1 = \frac{1}{j\omega_0\lambda_0}[I_{p0}V_1 - I_{p1}V_1^*] \tag{11}$$

since $i_l(t) = i_p(t)/\lambda_0 \int v_l\,dt$. Using the circuit model or the small-signal linearized form of (1)–(3), the diode voltage V_d at ω_0 is then

$$V_d = V_1 + \frac{1-\beta}{j\omega_0 C} I_1 = V_1\left(1 - \frac{1-\beta}{\omega_0^2\lambda_0 C} I_{p0}\right) + \frac{1-\beta}{\omega_0^2\lambda_0 C} I_{p1}V_1^* \tag{12}$$

with $\beta = [1 - \exp(-j\omega_0\Upsilon)]/j\omega_0\Upsilon$. The total diode current at ω_0 is likewise

$$I_d = \beta I_1 + j\omega_0 C V_d. \tag{13}$$

Using (11) and (12) in (13), the diode "subharmonic admittance" as pumped can be defined as

$$Y_d(\omega_0,\theta_1,I_{p1}/I_{p0}) \triangleq \frac{I_d}{V_d} = j\omega_0 C + \beta \frac{1 - (I_{p1}/I_{p0})\exp(-2j\theta_1)}{j(\omega_0\lambda_0/I_{p0}) + (1-\beta)/j\omega_0 C(1 - (I_{p1}/I_{p0})\exp(-2j\theta_1))} \tag{14}$$

where θ_1 is the angle of V_1, i.e., $V_1 = |V_1| \exp(j\theta_1)$. This quantity is not an admittance in the normal sense as it is dependent on the phase angle between the fundamental pumping current and the small-signal subharmonic voltage V_1 across the nonlinear inductor. Subharmonic oscillations will then occur if the circuit admittance $Y_c(\omega_0)$ satisfies the normal oscillation condition

$$Y_c(\omega_0) = -Y_d(\omega_0,\theta_1,I_{p1}/I_{p0}) \tag{15}$$

for any value of θ_1, $0 \le \theta_1 \le z\pi$, and pumping level. A solution to (15) for any value of pumping at ω_p may be possible with many values of circuit admittance, each corresponding to a different value of θ_1. As a function of θ_1 with constant pumping, Y_d from (14) traces a circular locus in the complex plane as can be seen from rearranging (14) and taking magnitudes as

$$\left|\frac{\beta - (Y_d - j\omega_0 C)[j\omega_0 L + (1-\beta)/j\omega_0 C]}{\beta - [(1-\beta)/j\omega_0 C](Y_d - j\omega_0 C)}\right| = \left|\frac{I_{p1}}{I_{p0}}\exp(-2j\theta_1)\right| = p \tag{16}$$

where the dc bias current I_{p0} is assumed constant and thus $L \triangleq \lambda_0/I_{p0}$ is a constant inductance independent of pumping level. At any nonzero value of p, the locus of Y_d for all possible phases θ_1 from (14) or (16) is a circle with center Y_{dp} and radius R_p given by

$$Y_{dp} = j\omega_0 C - \beta\frac{[(1-\beta^*)/j\omega_0 C](1-p^2) + j\omega_0 L}{|(1-\beta)/j\omega_0 C + j\omega_0 L|^2 - p^2|(1-\beta)/j\omega_0 C|^2} \tag{17a}$$

$$R_p = \left|\frac{\omega_0 L\beta p}{|(1-\beta)/j\omega_0 C + j\omega_0 L|^2 - p^2|(1-\beta)/j\omega_0 C|^2}\right| \tag{17b}$$

that is

$$|Y_d - Y_{dp}| = R_p \tag{18}$$

is equivalent to (16) or (14) as a function of θ_1. If the negative of the circuit admittance $-Y_c$ lies on the circle defined by (18), a subharmonic oscillation will begin at pumping level p, with V_1 having the appropriate phase from (14). The phase of V_1 is not unique, but may have one of two possible values 180° apart since two such phases will give the same Y_d. The oscillation will be phase locked to the pump and not subject to random phase modulation [1]. Further, since Y_c is a positive-real admittance, the locus of Y_d at some values of p must lie at least partly in the negative-real half of the complex plane for (15) to ever be satisfied.

In the limit of low pumping, p and R_p approach zero and $Y_d \to Y_{dp}$ $(p = 0)$ which is the *small-signal unpumped diode admittance at* ω_0. Normally, this will have a positive-real part since the small-signal avalanche frequency will generally be greater than ω_0 but less than ω_p. A free oscillation cannot occur at ω_0 under this condition. As the device is pumped, p and R_p increase and Y_{dp} changes. From observations of subharmonic generation, one expects that Y_d from (18) will eventually lie partly in the left half-plane and (15) may be satisfied at some pumping level or *threshold*. Thus, by determining the locus of $Y_d(p)$ to high pumping levels, one can specify those values of Y_c to avoid if subharmonic generation and fundamental frequency power robbing are to be prevented.

If $-Y_c$ lies inside a circle defined by (18), then the oscillation will grow with time and the small-signal equations will become invalid. As will be shown, the oscillation con-

ditions would be satisfied at some reduced pumping level where oscillation would begin; further drive is then likely to increase the power extracted by the subharmonic at the expense of the fundamental.

As pointed out in [4], $i_p(t)$ from (4) is always positive and consequently $p = |I_{p1}/I_{p0}| \leq 1$ for any pumping voltage waveform. We therefore define the limit circle as the one occurring at $p = 1$ in (17). Using the short transit angle approximation [3], [10] (usually valid at $\omega_p/2$) the limit center Y_{dl} and limit radius R_{dl} have the convenient form

$$Y_{dl} = j\omega_0 C + \frac{1}{j\omega_0 L} - \frac{\Upsilon}{2L} \tag{19a}$$

$$R_{dl} = \left| \frac{1}{j\omega_0 L} - \frac{\Upsilon}{2L} \right|. \tag{19b}$$

The limit circular locus passes through the point $Y_d = j\omega_0 C$, encloses the origin, and lies substantially in the negative-real half of the complex plane. Further, since $dR_p/dp > |dY_{dp}/dp|$, $0 \leq p \leq 1$ from (17), the limit circle *encloses all other circles* for any $p < 1$ and thus (19) or (17) at $p = 1$ can be taken to define the region in the complex plane to be avoided by $-Y_c$. Using (15), (18), and (19) for short transit angles the condition on Y_c for subharmonic suppression is then written as

$$\left| Y_c + j\omega_0 C + \frac{1}{j\omega_0 L} - \frac{\Upsilon}{2L} \right| > \left| \frac{1}{j\omega_0 L} - \frac{\Upsilon}{2L} \right|, \qquad \mathrm{Re}\{Y_c\} > 0 \tag{20}$$

and interpreted graphically in Fig. 2 with the shaded region to be avoided. Since $1/(LC)^{1/2}$ is very nearly the avalanche frequency ω_a and usually $\omega_0 < \omega_a$, the center of the shaded region will generally be in the upper half-plane. This implies a *low* shunt inductance across the diode at ω_0 would be desirable. This is in partial agreement with the results of [4], although any *large* admittance would be equally effective in eliminating subharmonics.

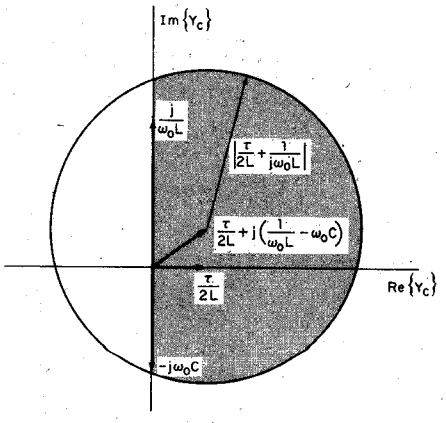

Fig. 2. The region of the complex plane to be avoided by the circuit admittance Y_c for prevention of second-subharmonic oscillations at any pumping ω_p.

We now present measured data on K_a-band IMPATT diodes which substantiates the theoretical predictions.

III. MEASUREMENT OF SUBHARMONIC ADMITTANCE AS PUMPED

The desired measurements were accomplished using the system shown in Fig. 3. This system provides a variable power pump source at f_p to an IMPATT amplifier in addition to a variable-phase measuring signal at $f_p/2$ which is phase locked to the pump. The measurement signal is in fact provided by harmonic division (second-subharmonic generation) using an active IMPATT diode network. The bandpass filters reject the fundamental from the slotted-line measuring system. For silicon diodes the IMPATT amplifier circuit used is that shown in Fig. 4 and has been described elsewhere [8]. Generally, no subharmonics limited the added power of this amplifier. The same circuit with an adjustable backshort was used for the GaAs diode

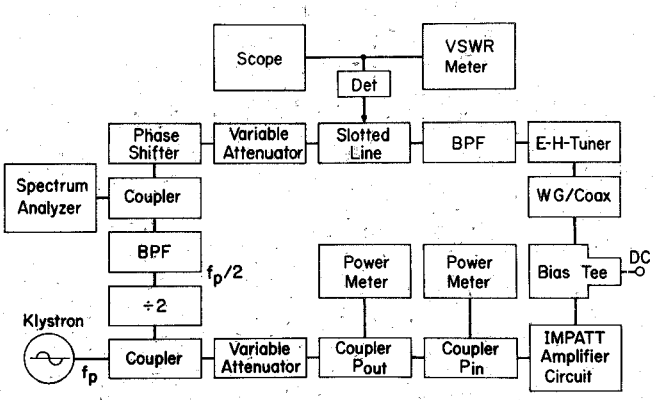

Fig. 3. Measurement system used to determine the second-subharmonic characteristics of pumped-silicon and GaAs IMPATT diodes.

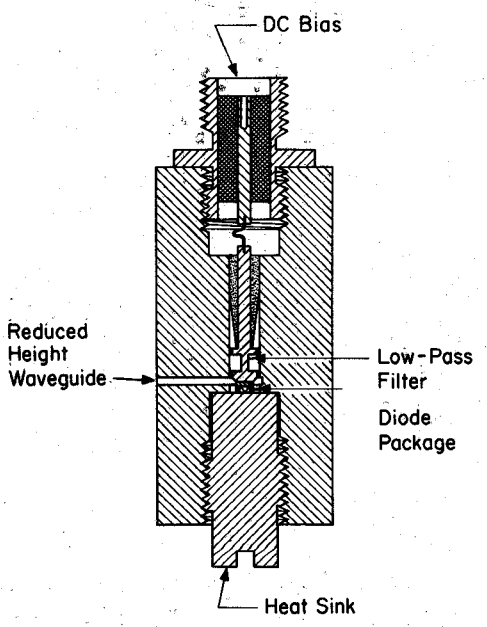

Fig. 4. IMPATT diode amplifier circuit. The backshort position shown is for silicon diodes; the backshort position on the GaAs circuit was variable.

measurements [11]. Subharmonic measurements were made into the bias port of these amplifier circuits with the bias line load (absorber) removed. The *E–H* tuner was used to provide adequate coupling to the diode and control the subharmonic oscillation thesehold.

With the measurement signal fully attenuated and the IMPATT biased, the pump power was increased from zero until a subharmonic or other parametric oscillation was observed on the standing wave ratio (SWR) meter. The unwanted parametric oscillations would occur 1–2 GHz above and below the half-frequency and were nearly degenerate. These effects would occur before the device was fully driven and could only be eliminated at the sacrifice of adequate coupling to the diode. Therefore, measurements at $f_p/2$ could only be made for pump powers below these thresholds. With no pump power to the diodes, measurements were made for several biases from 0 V to breakdown and then to a desired avalanche current. These measurements were used for de-embedding and determining device circuit model parameters as described in [10]. Then at the prescribed avalanche current, pump power was applied and held constant while measurements were made for several different signal phases. The largest pump power used was just below the threshold previously described. The measurement signal level was typically around 20 μW.

Measured data for silicon and GaAs devices are shown in Figs. 5 and 6, respectively. The circular loci are the results of phase variation of the measurement signal at constant pump power. Since the coupling network between the measurement reference plane and the diode provides a bilinear transformation of admittance these loci map to circles in the diode admittance plane. Further, since the inside of the circle formed by extending the varactor region arc is the mapping of all passive diode admittances, the data shows that although the diode is passive at the dc operating current when unpumped, small pumping will result in negative-real device admittance for some signal phases as espected. The circle radius increases with pumping and the highest pumping circle captures all lower pumping circles.

Using the varactor region data and 1-MHz capacitance measurements, the data of Figs. 5 and 6 were de-embedded and the results are shown in Figs. 7 and 8. The small-signal admittance and pumping circles were predicted for each diode from theory after determining the equivalent model parameters, C, Υ, and λ_0 for these devices. These model parameters were determined by matching the equivalent circuit admittance to the de-embedding admittance at the dc operating current and taking C as the breakdown capacitance from 1-MHz measurements. The equivalent parameters used for the theoretical predictions are also given in Figs. 7 and 8.

The circles of empirical data have centers that decrease in both conductance and susceptance with increasing pump power, agreeing with predictions of (17), and a substantial portion of these circles lies in the left half-plane even at low pumping. At low pumping the circle radii should increase approximately proportional to the square

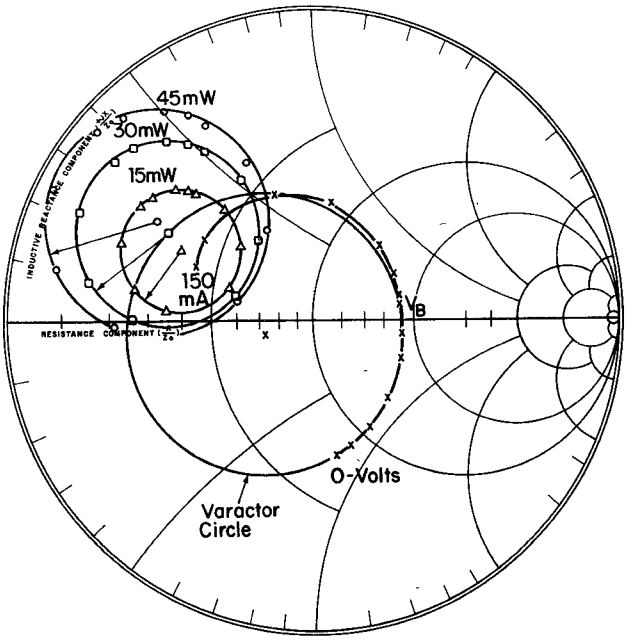

Fig. 5. Measured characteristics of the silicon diode of an arbitrary reference plane before de-embedding. The frequency is 18.75 GHz.

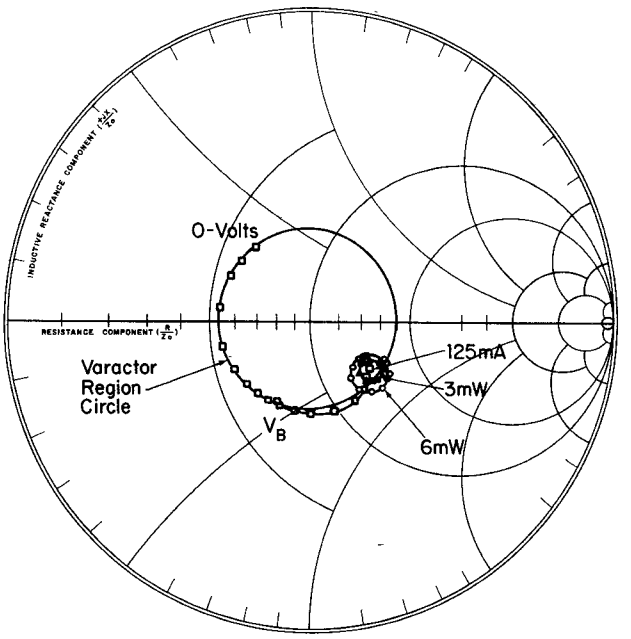

Fig. 6. Measured characteristics of the GaAs diode of an arbitrary reference plane before de-embedding. The frequency is 18.75 GHz.

root of RF added power as is also observed in Figs. 7 and 8. The predictions of subharmonic admittance based on the assumed device model with readily determined experimental parameters are seen to be in good quantitative agreement with measured results for the diodes investigated. Although the limit circle and actual values for $p = |I_{p1}/I_{p0}|$ were not determined experimentally,[2] the

[2] Finding actual values of p would require accurate de-embedding at 37.5 GHz so that device quantities (RF voltage or current amplitude and impedance) can be determined from measured quantities (RF input power and scattering coefficient). This was not carried out because poor coupling to the below-breakdown capacitance at K_a band would not allow accurate de-embedding.

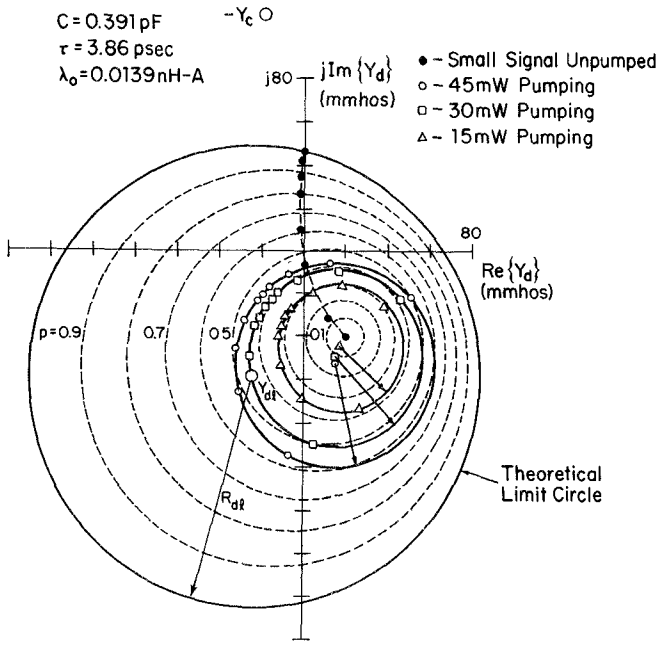

Fig. 7. De-embedded characteristics of the silicon diode. Solid lines are drawn for measured data. Dashed lines are theoretical predictions of the equivalent model shown. Model parameters were determined from small-signal unpumped data.

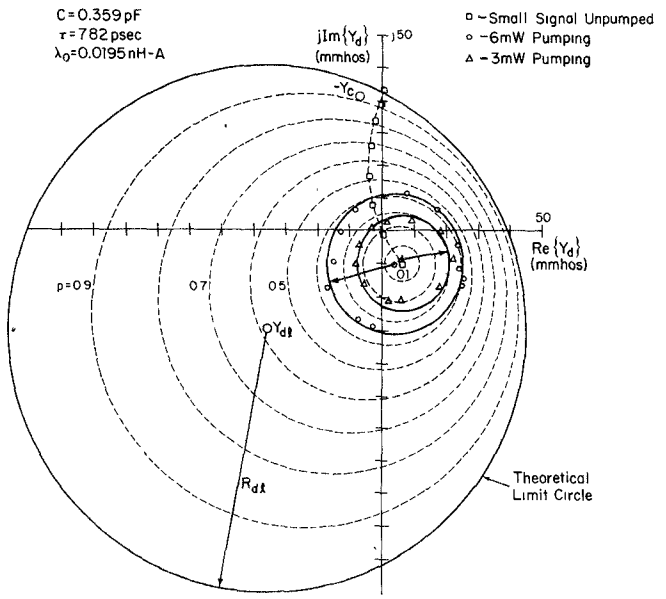

Fig. 8. De-embedded characteristics of the GaAs diode. Solid lines are drawn for measured data. Dashed lines are theoretical predictions of the equivalent model shown. Model parameters were determined from small-signal unpumped data.

trends between measured and predicted results are the same and indicate that the underlying assumptions to obtain (17) are reasonable.

Also shown in Figs. 7 and 8 are the negative circuit admittances at the subharmonic for both the silicon and GaAs normal amplifier circuits. The close-in backshort position of the silicon circuit tends to produce a low shunt inductance across the diode and subharmonics did not limit the added power of these amplifiers. The circuit for GaAs diodes required a further out backshort position for stability at the fundamental, and thus the low inductive

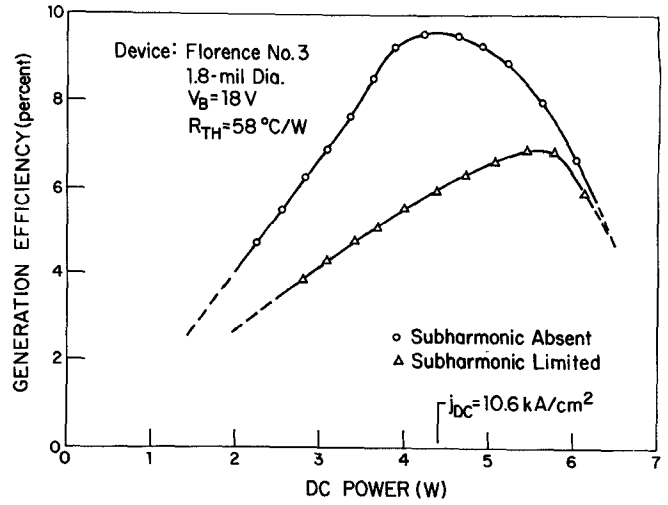

Fig. 9. Generation efficiency of a GaAs IMPATT diode amplifier at 37.5 GHz as a function of dc input power. The lower curve is limited by the onset of subharmonics at some RF drive power below that which results in maximum added power.

shunting effect was eliminated and subharmonics were observed in these amplifiers at moderate drive levels. For these amplifiers, the subharmonics were effectively eliminated by increasing the device package capacitance to provide a series resonance to the diode at 18–19 GHz and shunt out the high impedance of the bias line. The effect of this circuit modification on the generation efficiency (added power efficiency) of the GaAs IMPATT amplifiers is shown in Fig. 9. These efficiency curves were generated, using the diode as an amplifier at 37.5 GHz, by finding the *maximum* in added power as a function of RF drive power at several values of dc input power obtained by constant current bias. This technique was previously described in [8] and the efficiency so obtained is independent of amplifier gain (the gain in this case was between 3 and 5 dB), but it can be easily controlled while retaining maximum generation efficiency [8]. From the graph it is readily apparent that the onset of subharmonics can severely limit the power-generating capability of an IMPATT diode, in this case a factor of 2 in efficiency. The GaAs devices used in the experiments have been previously described in [11].

IV. SUMMARY AND CONCLUSIONS

Threshold conditions for subharmonic oscillation in driven IMPATT diode networks have been determined theoretically from a reasonable model of the device nonlinearity. Small-signal subharmonic measurements performed on pumped K_a-band silicon and GaAs devices yield results that behave in the manner indicated by theory and also agree quantitatively with the equivalent model predictions. Accordingly, through a few simple device measurements to determine appropriate model parameters, the designer of IMPATT amplifiers and oscillators can determine and design the correct network at $f_p/2$ to prevent subharmonic power extraction from the fundamental. It was shown that generally any large admittance is desirable at $f_p/2$, although the designer can choose from a wide

range of values to ease the circuit design and realization problem.

REFERENCES

[1] P. Penfield and R. Rafuse, *Varactor Applications*. Cambridge, Mass.: M.I.T. Press, 1962.
[2] W. T. Read, Jr., "A proposed high frequency negative-resistance diode," *Bell Syst. Tech. J.*, vol. 37, pp. 401–446, Mar. 1958.
[3] W. J. Evans and G. I. Haddad, "A large signal analysis of IMPATT diodes," *IEEE Trans. Electron Devices*, vol. ED-15, pp. 708–717, Oct. 1968.
[4] M. E. Hines, "Large-signal noise, frequency conversion, and parametric instabilities in IMPATT diode networks," *Proc. IEEE*, vol. 60, pp. 1534–1548, Dec. 1972.
[5] C. P. Snapp, "Subharmonic generation in the trapped-plasma mode in avalanching silicon p^+-n-n^+ junctions," *IEEE Trans. Electron Devices*, vol. ED-18, pp. 294–308, May 1971.
[6] W. E. Schroeder and G. I. Haddad, "Effect of harmonic and subharmonic signals on avalanche-diode oscillator performance," *IEEE Trans. Microwave Theory Tech.* (Corresp.), vol. MTT-18, pp. 327–331, June 1970.
[7] W. E. Schroeder, "Nonlinear properties of IMPATT diodes," Ph.D. dissertation, Univ. Michigan, Ann Arbor, 1972.
[8] D. F. Peterson, "A device characterization and circuit design procedure for realizing high-power millimeter-wave IMPATT-diode amplifiers," *IEEE Trans. Microwave Theory Tech.*, vol. MTT-21, pp. 681–689, Nov. 1973.
[9] D. F. Peterson and D. H. Steinbrecher, "Circuit model for characterizing the nearly linear behavior of avalanche diodes in amplifier circuits," *IEEE Trans. Microwave Theory Tech.*, vol. MTT-21, pp. 19–27, Jan. 1973.
[10] D. H. Steinbrecher and D. F. Peterson, "Small-signal model with frequency-independent elements for the avalanche region of a microwave negative-resistance diode," *IEEE Trans. Electron Devices*, vol. ED-17, pp. 883–891, Oct. 1970.
[11] R. A. Murphy *et al.*, "Proton guarder GaAs IMPATT diodes," presented at the 1972 Symp. Gallium Arsenide.

Short Papers

Further Experiments Seeking Evidence of Nonthermal Biological Effects of Microwave Radiation

G. A. LINDAUER, MEMBER, IEEE, L. M. LIU, G. W. SKEWES, AND F. J. ROSENBAUM, SENIOR MEMBER, IEEE

***Abstract*—Carpenter and Livstone's [1] experiments on beetle pupae are repeated and extended. In the experiments conducted, increased incidence of abnormal development occurred due to exposure to microwave energy, both CW and pulsed. This effect was observed at the power level of 8.6 mW/cm². Measurements are reported which specify the microwave environment encountered by the insect.**

I. INTRODUCTION

This short paper reports experiments undertaken to verify and augment the observations of Carpenter and Livstone [1] on teratological damage inflicted upon the darkling bettle *Tenebrio molitor* by low power microwave irradiation.

We first repeated the Carpenter and Livstone study in waveguide at the 20-mW CW irradiation level with a much larger sample population and, having confirmed their results, conducted experiments in which individual experimental parameters—duty cycle, orientation, pupa age, power level, and total absorbed energy—were varied in a phenomenological approach to elucidate mechanisms by which teratological damage is realized. Finally, measurements were made to specify the microwave environment encountered by the insect.

II. EXPERIMENT

One- to two-day-old pupae (nominally, 3/16-in diameter × 5/8-in length) were mounted for irradiation in styrofoam blocks, then inserted along the center line of X-band waveguides with their anterior portions towards the power source as shown in Fig. 1 The waveguide was terminated in a matched load. The pupae were irradiated at 9 GHz, then placed for the duration of pupation in individual numbered vials in a darkened chamber at 21°C. The emergent adults were categorized for gross morphological defects as per the scheme of Carpenter and Livstone in ignorance of whether a particular insect was from the irradiated or control group ("single-blind").

No attempt was made to impedance match the pupa and holder, in contrast to the method of Carpenter and Livstone. The combined mismatch was considered small with less than 5.1 percent of the incident power being reflected (13-dB return loss). Also the introduction of a matching element would distort the field distribution in the vicinity of the pupa, thereby further complicating interpretation of field strength measurements.

Waveguide was chosen as the experimental environment to conform with the original experiments of Carpenter and Livstone, In addition, a waveguide apparatus allows the precise determination of incident and reflected power levels, and of the power absorbed by the specimen.

A diagram of the microwave circuit used for the simultaneous irradiation of four pupae is shown in Fig. 2. An 80-mW CW Gunn oscillator was the microwave source. The power incident on each pupa was 20 mW, which is equivalent to a power density of 17.1 mW/cm², at the center of the X-band waveguide. Free space radiation at a power density of 17.1 mW/cm² could be obtained using a 1-W source and a horn antenna with an aperture of 0.90 in × 0.90 in at a distance of 4.93 cm from the horn. The 1-dB beamwidth of this horn would accommodate five pupae spaced on a 1/2-in center in a triangular grid. Thus waveguide irradiation requires much less source power than free space irradiation at the same power density.

Since the experiments were done in waveguide, it is of interest to consider effects present there which might modify free space irradiation results. One such effect is the excess attenuation obtained in a waveguide partially loaded with a lossy dielectric medium which can exceed that of the same waveguide completely filled with the same material [2]–[4]. This excess loss is due to field concentration effects and could lead to a greater temperature rise in the pupa than anticipated.

The temperature rise due to microwave power absorption was monitored by imbedding a fine copper-constantan thermocouple (0.005-in wire) in the abdomen of sample pupae. The leads were brought out through small lateral channels in the flange of the X-band waveguide section. The leads were perpendicular to the electric field vector to minimize induced currents in the thermocouple. A reference junction was mounted in an identical styrofoam

Manuscript received August 25, 1973; revised April 10, 1974. This work was supported by the U. S. Public Health Services, Grant HSAA-5504-FR-06115-05, and the Biomedical Sciences Support Grant BSSG-RR07054.

G. A. Lindauer was with the Department of Electrical Engineering, Washington University, St. Louis, Mo. 63130. He is now with Emerson Electric, St. Louis, Mo. 63136.
L. M. Liu, G. W. Skewes, and F. J. Rosenbaum are with the Department of Electrical Engineering, Washington University, St. Louis, Mo. 63130.